Electronic Supplementary Information for

Hydroxide Transport and Chemical Degradation in Anion Exchange Membranes: A Combined Reactive and Non-reactive Molecular Simulation Study

Weiwei Zhang[a], Dengpan Dong[b], Dmitry Bedrov[b*], and Adri C. T. van Duin[a*]

[a]*Department of Mechanical and Nuclear Engineering, Pennsylvania State University, University Park, Pennsylvania 16802, United States*

[b]*Department of Materials Science and Engineering, University of Utah, Salt Lake City, Utah 84112, United States*

*E-mail: acv13@psu.edu, d.bedrov@utah.edu,

Tracking OH-anion in ReaxFF:

In order to obtain the structural and transport properties referring to OH^- anion, the index of oxygen (O*) of the hydroxide ion should be monitored and distinguished from water molecules because the index of O* may change due to the proton transport from water molecule to hydroxide anion.[1-3] The same index of O* between two adjacent frames in simulation trajectory indicates no proton transport. When the index changes it indicates that the Grotthuss hopping or transport occurs.

RDF and CN calculations:

In order to investigate the structural properties of AEMs, we calculated the radial distribution function (RDF) and the coordination number of atom within a given radius shell[4]

$$g(r) = \frac{n(r)}{\rho 4\pi r^2 \Delta r}$$
$$CN = \int_0^{r'} \rho 4\pi r^2 g(r) dr, \qquad \text{(eq-S1)}$$

where $g(r)$ and CN are RDF and coordination number, respectively. $n(r)$ represents atoms number within a distance r of the central atom, ρ strands for the number density. r' is the cutoff distance for integration. The RDF and CN were obtained by averaging over the trajectory.

Diffusion constant:

From the time-dependent trajectory, the diffusion constant of OH^- or H_2O can be estimated from mean squared displacement (MSD)[5]

$$MSD(t) = \frac{1}{N} < \sum_{i=1}^{N} | r_i(t + t_0) - r_i(t_0)|^2 >, \quad \text{(eq-S2)}$$

where N is denoted the total number of atoms. r_i represents the position of the *i-th* atom in the unfolded trajectory, t_0 is the origin of time. With the time-dependent MSD, the diffusion constants were then estimated using the Einstein relation

$$D = \frac{1}{6t} MSD(t). \quad \text{(eq-S3)}$$

Here *N* is the number of OH^- or H_2O in the system.

Water channel size distribution:

The water channel sizes distribution is calculated based on the 'pore-size distribution' (PSD) concept with minor modifications.[6, 7] The diagram shown in Figure S2 illustrates the algorithm to calculate the water channel size distribution. Once the water channel boundary is defined, then the water channel size calculation is equivalent to calculating the distribution of spheres that can fit into the channel. Here, the water channel boundary is defined by isosurfaces with 25% of bulk water density. The potential locations for the centers of attempted sphere inscriptions is defined by the region where the water density is larger than 50% of bulk water density (i.e. the core of the water channel).

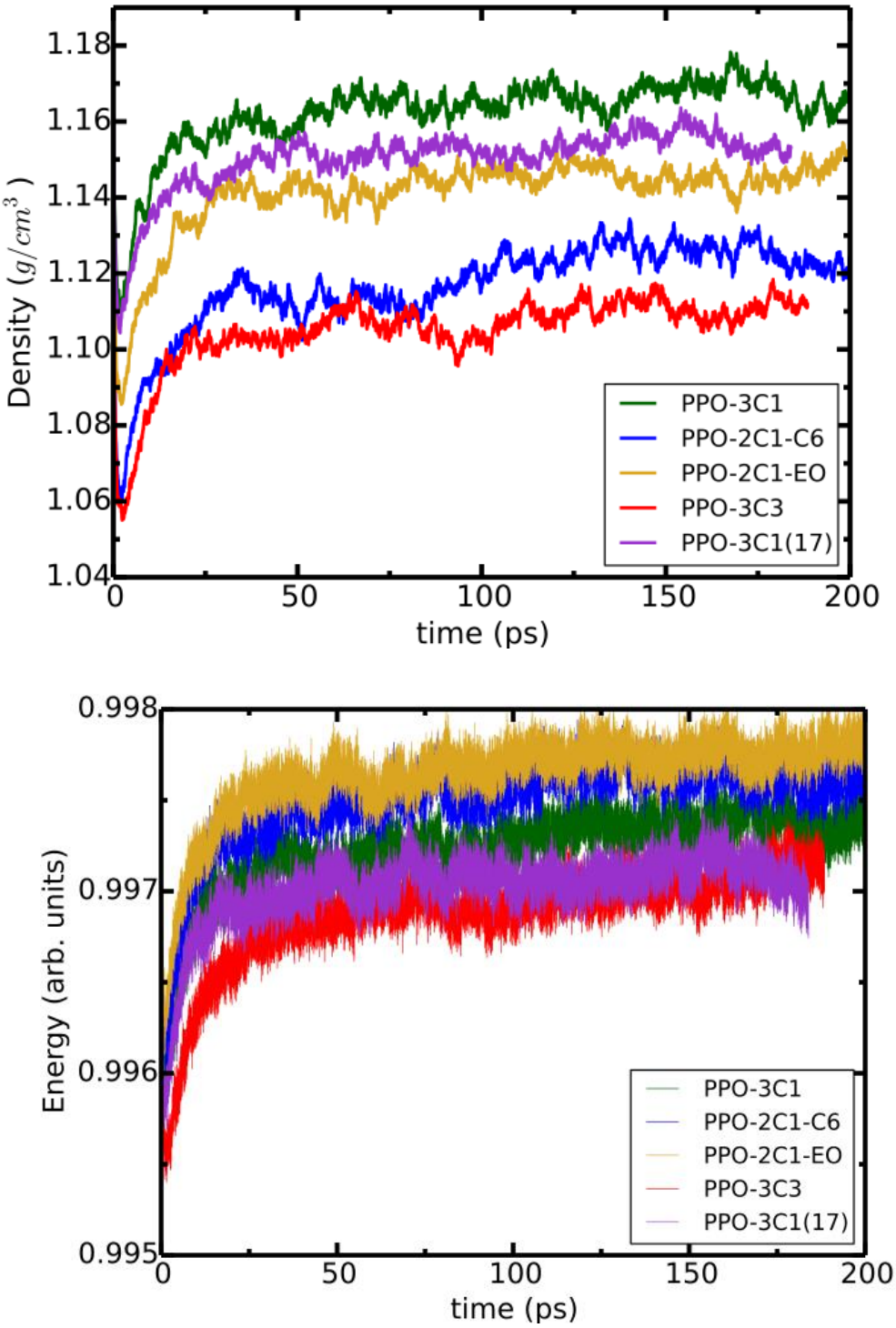

Figure S1. Time dependence of density and energy for all systems in ReaxFF simulations. The initial energy for each system is set to 1.00 when mapping from APPLE&P to ReaxFF. The hydration level is λ =17 for PPO-3C1(17) while it corresponds to λ =10 for others. From the results of density and energy, we show the systems are equilibrated.

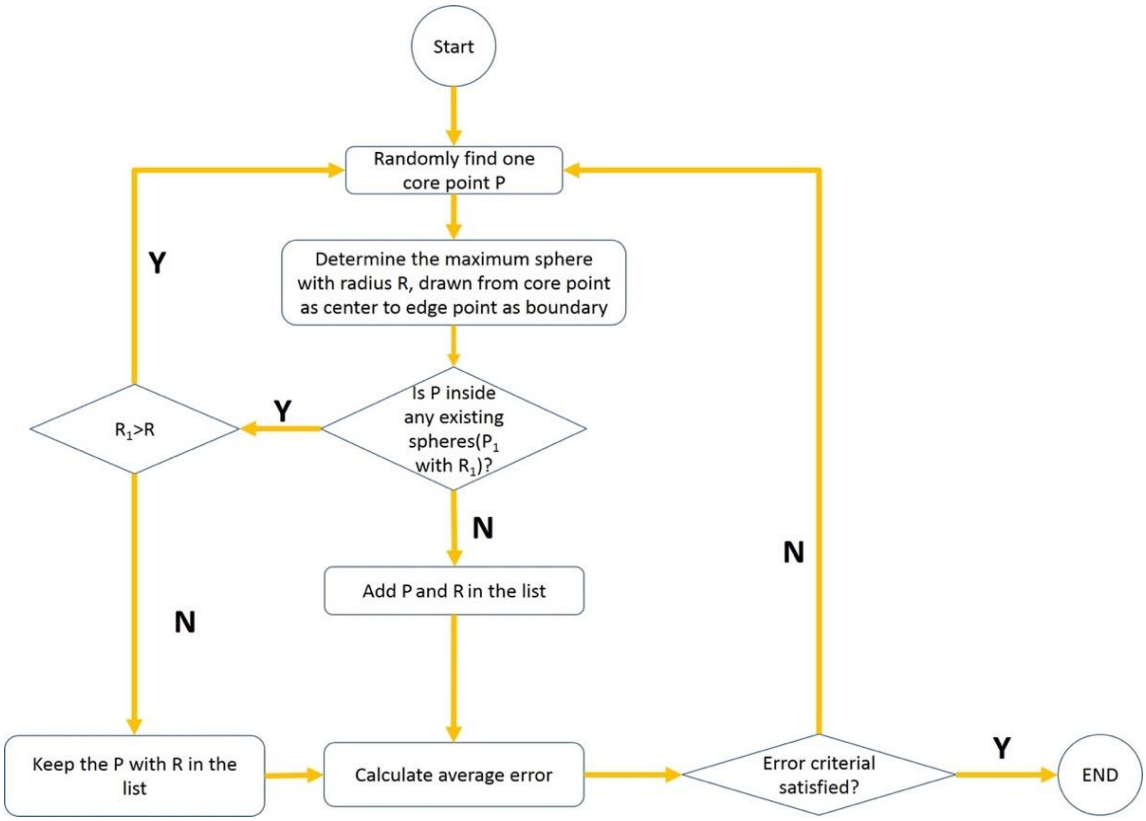

Figure S2. The algorithm for calculation the water channel size distribution.[7]

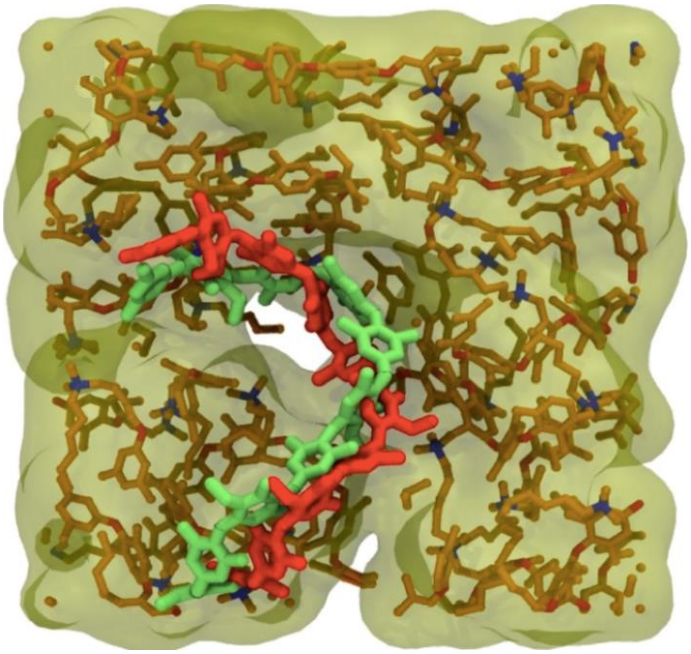

Figure S3. Illustration of PPO-2C1-C6 membrane morphologies obtained from APPLE&P and ReaxFF simulations. The red chain shows a polymer backbone for the selected chain in the APPLE&P simulation, while green chain shows the same chain after mapping and relaxation in ReaxFF.[7]

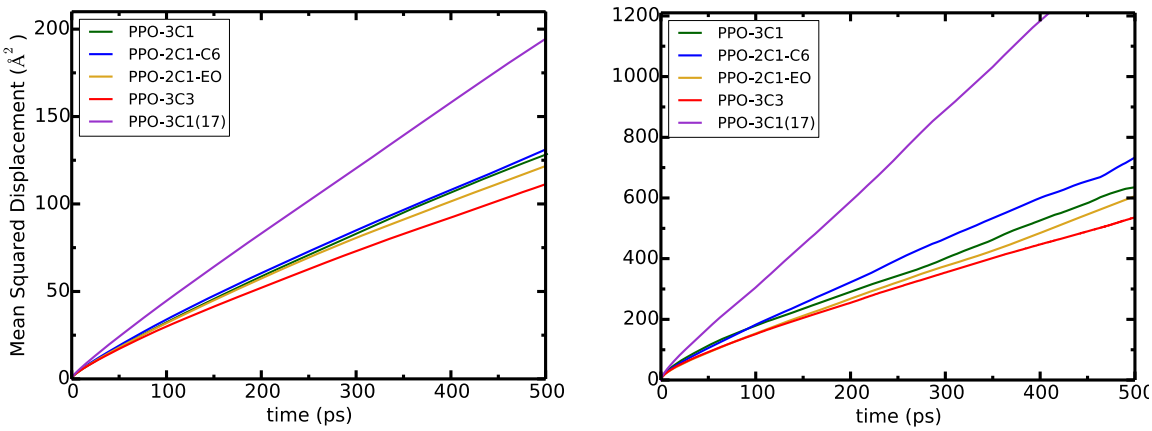

Figure S4. Mean squared displacement (MSD) of water (left) and OH-anion (right) obtained from ReaxFF simulations at hydration level λ =17 for PPO-3C1(17) and λ =10 for all other systems.

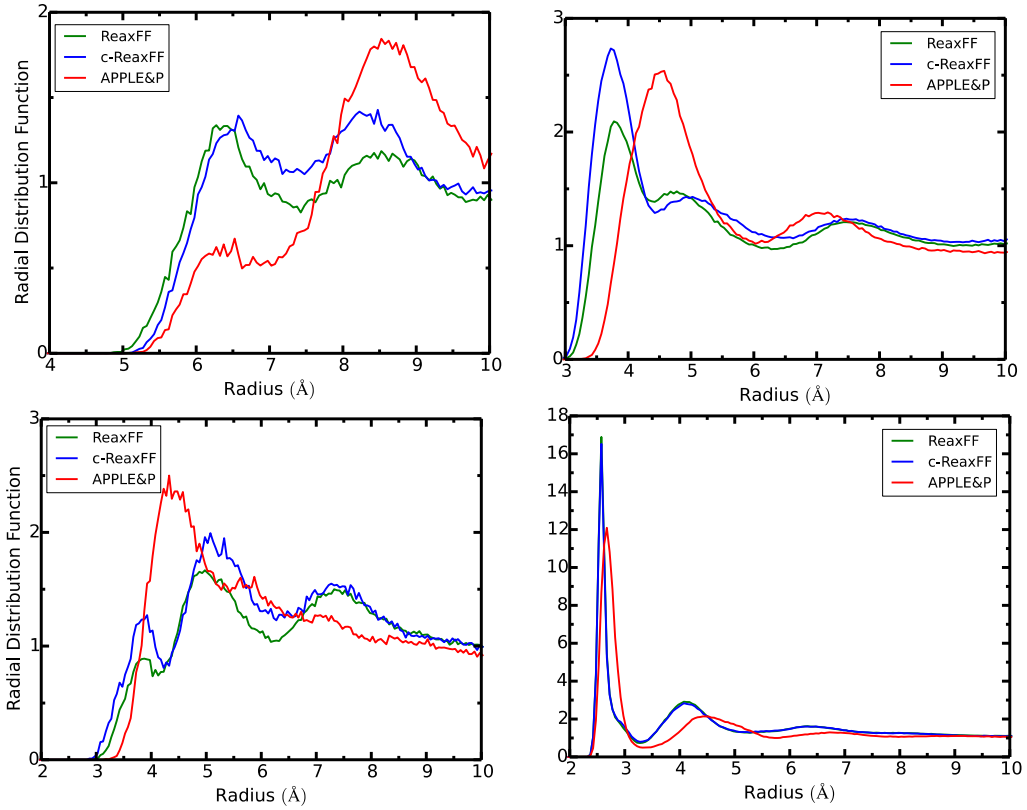

Figure S5. The RDFs of N-N (left, upper), N-O (H_2O) (right, upper), N-O^* (OH^-) (left, lower) and O^*-O (right, lower) predicted with APPLE&P, standard ReaxFF, and charge constrained ReaxFF simulations for the system of trimethylamines attached to p-phenylene oxide dimer(TPO)-OH anion-water.

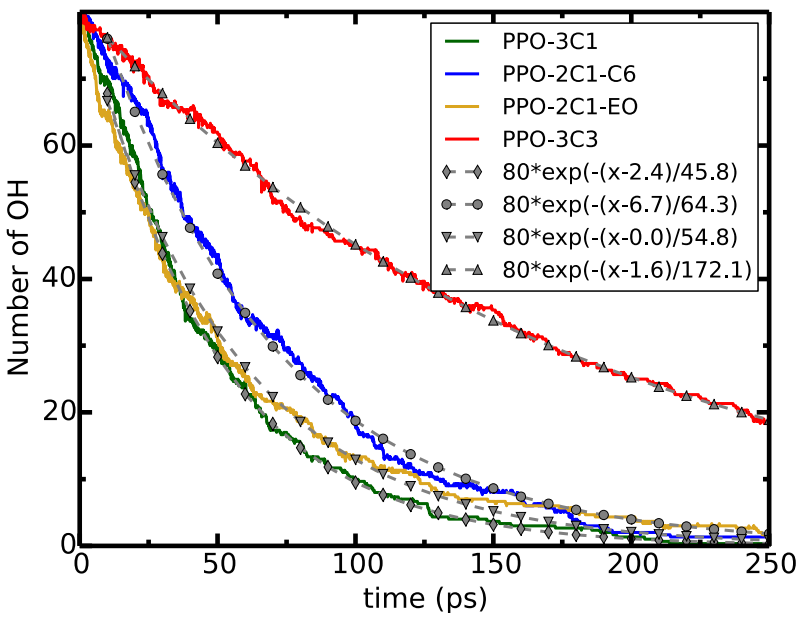

Figure S6. Time dependence of OH^- residual number in PPO-3C1, PPO-2C1-C6, PPO-2C1-EO and PPO-3C3 AEMs, as well as the two-parameter fitting curves.

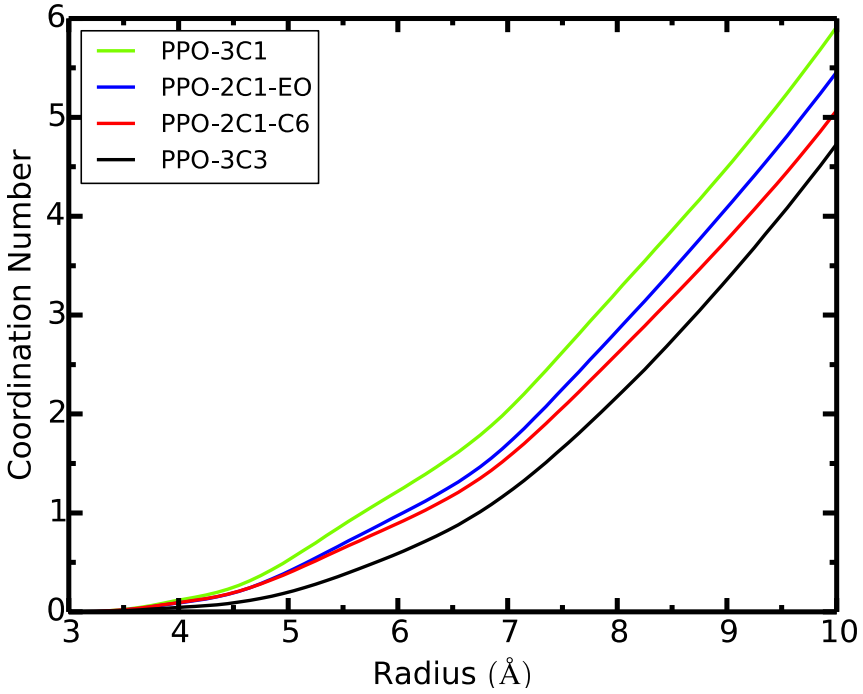

Figure S7. The coordination numbers of nitrogen-hydroxide in PPO-3C1, PPO-2C1-C6, PPO-2C1-EO and PPO-3C3 AEMs.

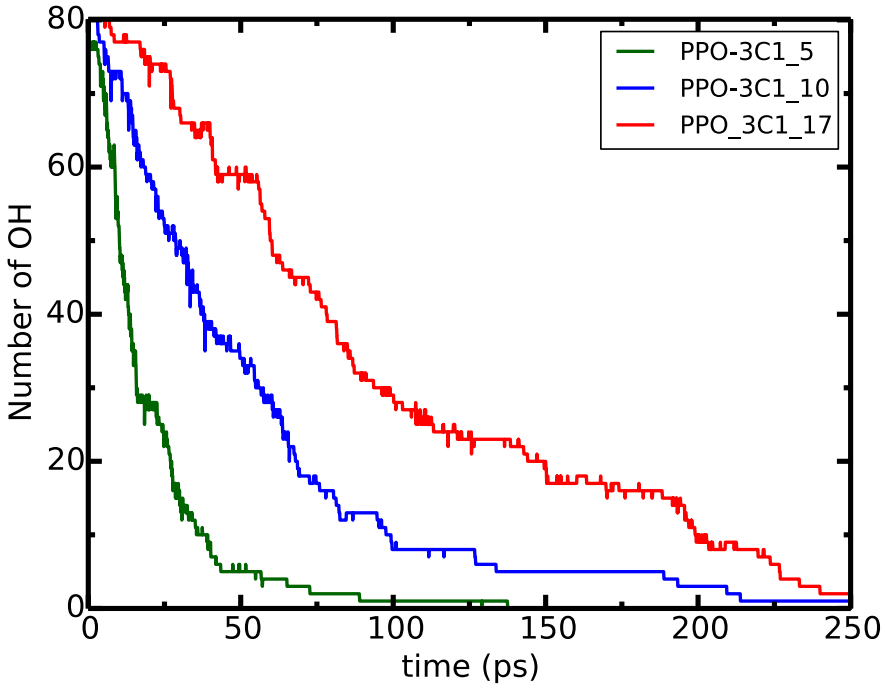

Figure S8. Time dependence of OH-anion residual number in PPO-3C1 at different hydration levels with 5, 10 and 17.

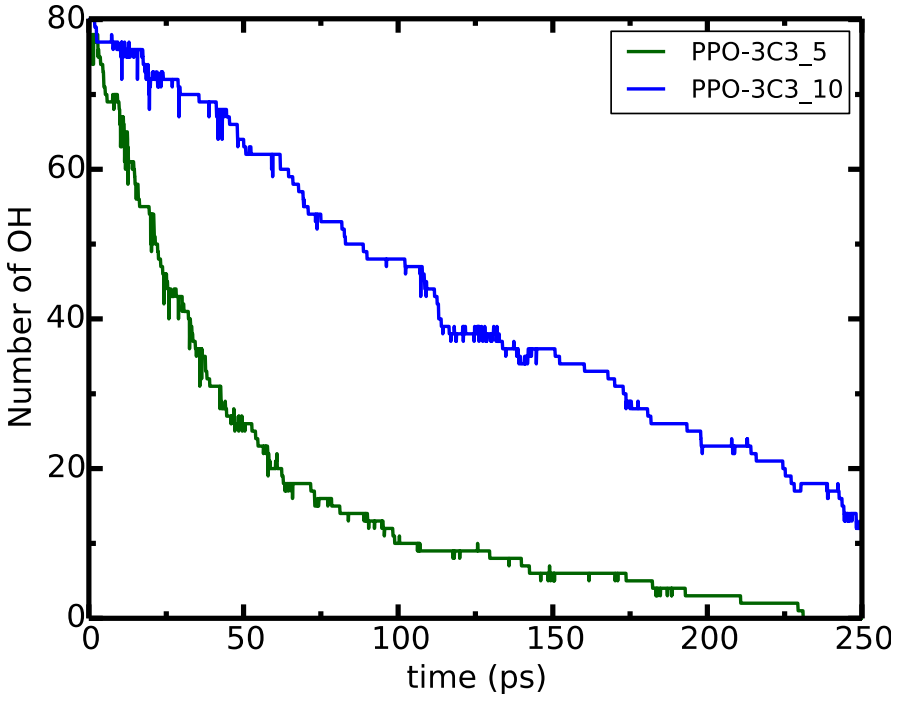

Figure S9. Time dependence of OH-anion residual number in PPO-3C3 at different hydration levels with 5 and 10.

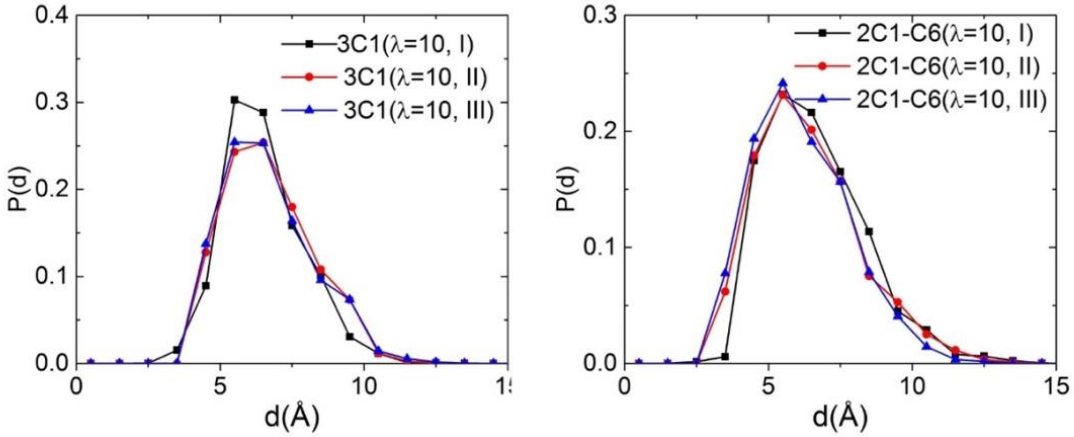

Figure S10. Distribution of water channel size of a given polymer at three different realizations of the membranes (PPO-3C1 and PPO- 2C1-C6).

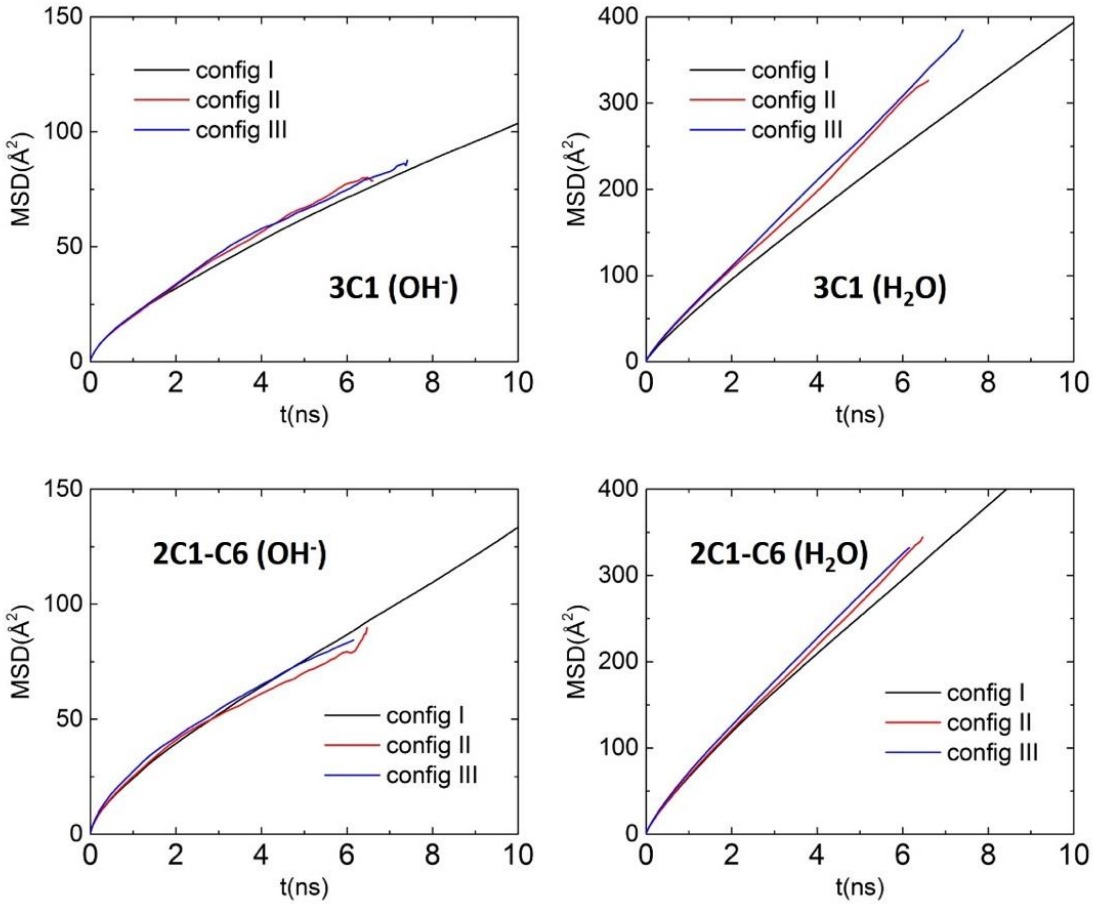

Figure S11. Mean squared displacements of OH^- and H_2O for different built polymer morphology (PPO-3C1 and PPO- 2C1-C6) at the hydration level of λ=10.

To quantify the correlation between D_{OH^-} and the distribution of water channel bottlenecks, we calculated the volume fraction of such bottlenecks in the formed channels.[8] A bottleneck region is defined as the portion of the water channel which can accommodate spheres with a radius less than 2.4 Å (big enough to fit an OH^-–H_2O pair) and larger than 1.5 Å (accommodate a single OH^-). The accumulated volume of these domains normalized by the total volume of water channels is a quantitative measure of the volume fraction of bottlenecks. The correlation between D_{OH^-} and the volume fraction of bottlenecks is shown in Figure S12A. It is clear that PPO-2C1-C6 with small volume fraction has the largest diffusion constant, indicating the co-existence of phase segregation and well-defined water channels enhance the dynamics of OH^-. However, for the point at 0.059, which corresponds to 3R3 polymer structure, D_{OH^-} increases with the decreasing volume fraction of bottleneck regions. Consistent with the enhanced phase segregation observed in the PPO-3C3 systems, the surface area of water channels defined by iso-surfaces with ρ/ρ_0 larger than 0.5 (i.e. larger than 50% of bulk density) is shown in Figure S12B. For any value defining the iso-surface, the PPO-3C3 system has the smallest surface area, indicating the formation of large water-rich domains and the limited interconnection between them. Therefore, the slow dynamics in the PPO-3C3 with a low volume fraction of bottlenecks can be attributed to the disconnection of water domains leading to the hindrance of OH^- transport from one water-rich domain to a neighboring one.

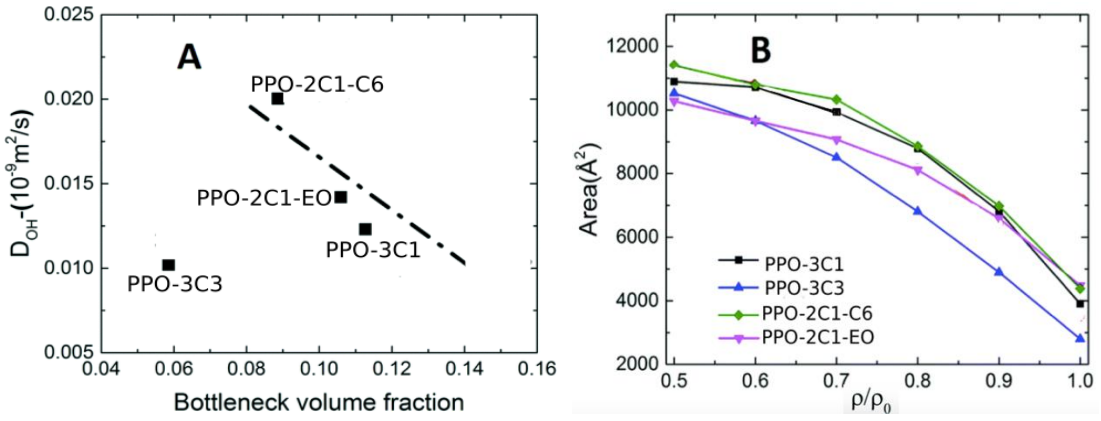

Figure S12: OH^- as a function of bottleneck volume fraction (A) and total surface area of the water channels as a function of isosurface density value used for defining water channels (B).[8]

Table S1. ReaxFF hopping rate (per OH^-/per ns) in different systems.

System	Hopping rate
PPO-3C1	5244
PPO-2C1-C6	5342
PPO-2C1-EO	5293
PPO-3C3	5353

The hopping rate of OH^- is calculated by normalizing the total number of proton hops by total time (in ns).

Table S2. The APPLE&P lifetime of hydrogen bonds for OH^- and water molecule in different AEMs (unit: ps).

AEMs	$OH^-(H_2O)_n$	$H_2O(H_2O)_n$
PPO-3C1	318.73	74.03
PPO-2C1-C6	305.75	42.85
PPO-2C1-EO	306.32	41.70
PPO-3C3	305.54	42.12
dilute water	13.51	2.05

Table S3. The simulated ionic conductivities in different AEMs (unit: $mS.cm^{-1}$).

AEM_S	APPLE&P	ReaxFF
PPO-3C1	1.1	176.3
PPO-2C1-C6	1.6	188.8
PPO-2C1-EO	1.1	146.2
PPO-3C3	0.65	118.3

Reference

1. S. H. Lee and J. C. Rasaiah, *The Journal of Chemical Physics*, 2011, **135**, 124505.
2. W. Zhang and A. C. van Duin, *The Journal of Physical Chemistry C*, 2015, **119**, 27727-27736.
3. W. Zhang and A. C. van Duin, *The Journal of Physical Chemistry B*, 2017, **121**, 6021-6032.
4. M. M. Islam, A. Ostadhossein, O. Borodin, A. T. Yeates, W. W. Tipton, R. G. Hennig, N. Kumar and A. C. van Duin, *Physical Chemistry Chemical Physics*, 2015, **17**, 3383-3393.
5. A. C. van Duin, B. V. Merinov, S. S. Han, C. O. Dorso and W. A. Goddard III, *The Journal of Physical Chemistry A*, 2008, **112**, 11414-11422.
6. S. Bhattacharya and K. E. Gubbins, *Langmuir*, 2006, **22**, 7726-7731.
7. D. Dong, W. Zhang, A. C. van Duin and D. Bedrov, *The Journal of Physical Chemistry Letters*, 2018, **9**, 825-829.
8. D. Dong, X. Wei, J. B. Hooper, H. Pan and D. Bedrov, *Physical Chemistry Chemical Physics*, 2018, **20**, 19350-19362.